Supporting Information

Self-Assembled Micro-Honeycomb Network of Single-Walled Carbon Nanotubes for Solar Cells

Kehang Cui, [1] *Takaaki Chiba,* [1] *Shuichiro Omiya,* [1] *Theerapol Thurakitseree,* [1] *Pei Zhao,* [1] *Shunjiro Fujii,* [2] *Hiromichi Kataura,* [2] *Erik Einarsson,* [1] *Shohei Chiashi,* [1] *Shigeo Maruyama*[1*]

[1] Department of Mechanical Engineering, The University of Tokyo, 7-3-1 Hongo, Bunkyo-ku, Tokyo 113-8656, Japan

[2] Nanosystem Research Institute, National Institute of Advanced Industrial Science and Technology, 1-1-1 Higashi, Tsukuba 305-8562, Japan

S1. Raman spectroscopy of as-synthesized and μ-HN of SWNTs

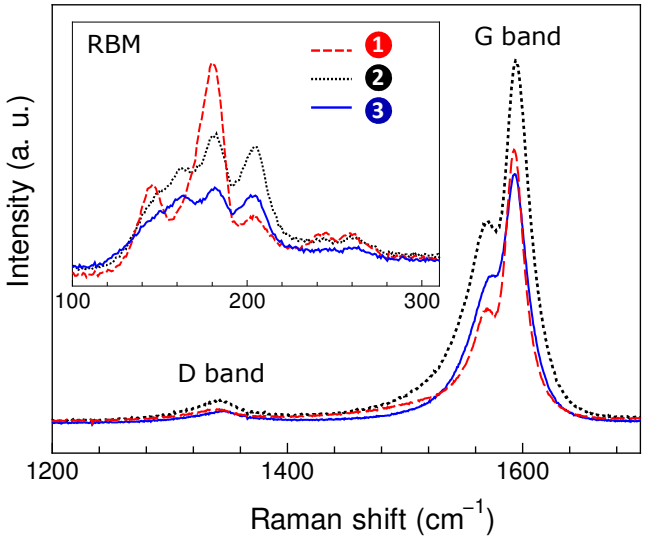

Figure S1. Resonance Raman spectra of SWNTs before and after water vapor treatment: spectrum 1 corresponds to as-synthesized VA-SWNTs. Spectra 2 and 3 correspond to the wall and bottom of the micro-honeycomb structure, respectively. All spectra were measured with a 488 nm excitation laser incident normal to the substrate.

Raman spectra were measured to characterize and compare the SWNT assemblies before and after water vapor treatment. Spectrum 1 in Figure S1 corresponds to as-synthesized VA-SWNTs, whereas spectra 2 and 3 were obtained from the highly condensed walls and buckypaper bottom, respectively. Spectrum 1 shows that the D-band is negligible for the as-synthesized VA-SWNTs, indicating the high quality and high purity of as-synthesized VA-SWNTs. Furthermore, the relative D-band intensity was nearly unchanged after water vapor treatment. This illustrates that the water vapor treatment did not induce defects in SWNTs. In the radial breathing mode (RBM) region (the inset of Figure S1), spectrum 1 has the characteristic of free-standing SWNTs, with strong peaks appearing at 181 cm^{-1}.[S1] The two characteristic peaks became much weaker after the water vapor treatment (spectra 2 and 3), owing to the morphology change of SWNTs. The reduction in peak intensity was more pronounced in the bottom of the honeycomb cell.

S2. Discussion on the μ-HN formation

The water reservoir temperature and the vapor exposure time are the two dominant factors determining the μ-HN formation. As the control, a 10 μL water droplet was dropped onto the top surface of a VA-SWNT film at room temperature. After evaporation of the water, the SWNTs had aggregated into a highly condensed bulk and generated many 100 μm-scale gaps (Figures S2-1a and S2-1b), which is in agreement with the report by Futaba *et al.* [S2] A similar phenomenon was observed for an ethanol droplet and an 80 ˚C water droplet. In the case of water vapor treatment, when the water reservoir temperature was increased to 50 ˚C, the length of the gaps decreased to ~50 μm and honeycomb cells started to form (Figure S2-2a). Further increase of the water reservoir temperature to 70 ˚C significantly reduced the size of the gaps to approximately 5 μm, and the size of honeycomb cells became more uniform (Figure S2-2b). A well-formed μ-HN was obtained when the water reservoir temperature reached 80 ˚C (Figure S2-2c). The vapor exposure time for the structures shown in Figures S2-2a, S2-2b and S2-3c was 5 s in all cases.

The effect of vapor exposure time on the morphology was investigated using a constant water reservoir temperature of 80 ˚C. Extending the exposure time from 2 s to 5 s resulted in an increase in micro-honeycomb cell size from ~2.5 μm (Figure S2-3a) to ~12 μm (Figure S2-3b). When the exposure time was longer than 15 s, the walls of the cells nearly disappeared, as most of the VA-SWNTs had collapsed as shown in Figure S2-3c. Compared with direct immersion or direct wetting (water droplet) [S3], water vapor treatment is a more delicate, controllable method.

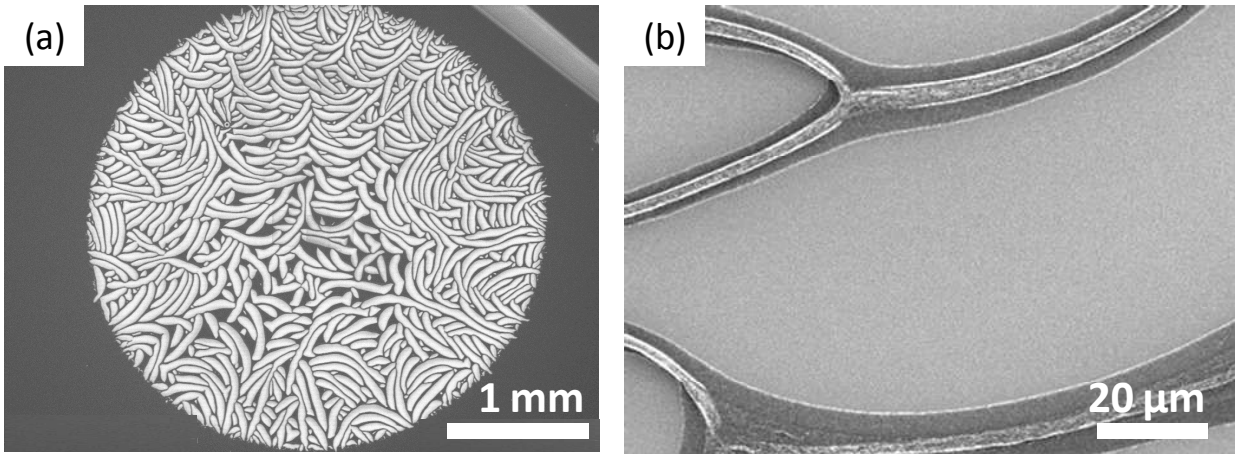

Figure S2-1. 100 µm-scale gaps obtained by applying a 10 µL water droplet to the surface at RT under (a) low magnification and (b) high magnification.

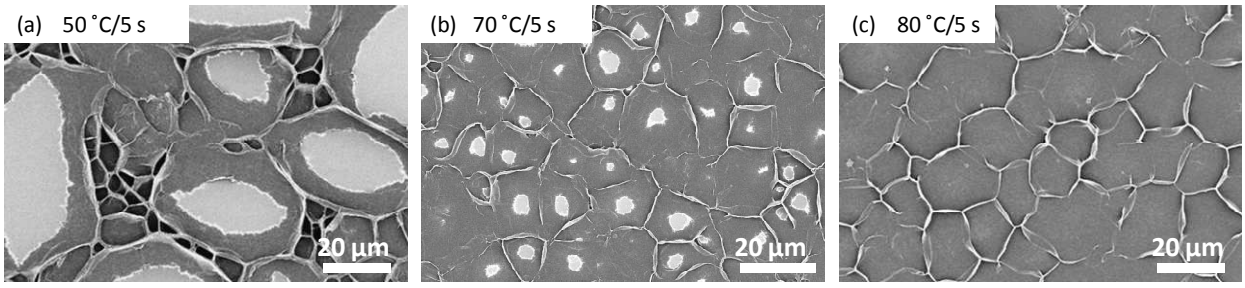

Figure S2-2. (a-c) Morphologies obtained by exposure to 50 ºC, 70 ºC and 80 ºC water reservoirs, respectively. The vapor exposure time for each vapor treatment step is 5 s.

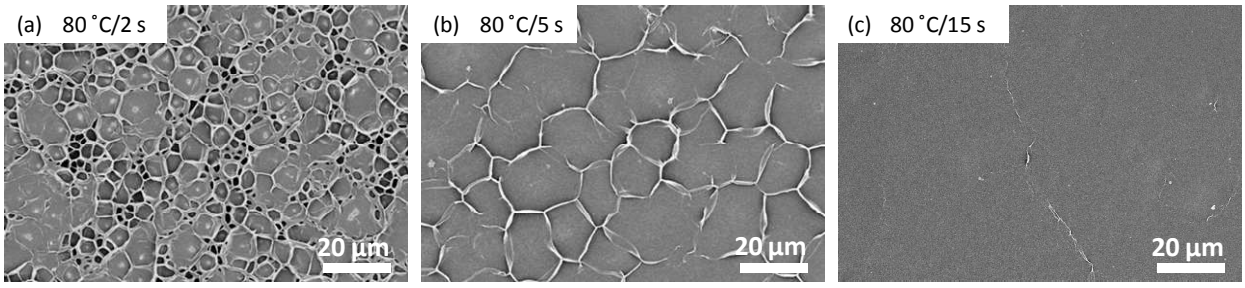

Figure S2-3. (a-c) Morphologies obtained with vapor exposure times of 2 s, 5 s and 15 s for each iteration, respectively. Reservoir temperature was 80 ºC.

S3. Effect of nitric acid treatment on the properties of μ-HN

To investigate the effect of nitric acid treatment on the morphology of μ-HN, we observed the SEM images, as shown in Figures S3-1a and S3-1b. The micro-honeycomb structure did not change as a whole, but the top of the walls appeared slightly compressed. The Raman spectra in Figure S3-2 show a 21 cm^{-1} upshift in both the G band and the G′ band as well as a significant increase in D band intensity. The Raman spectra further prove that the SWNTs samples are heavily *p*-doped[S4].

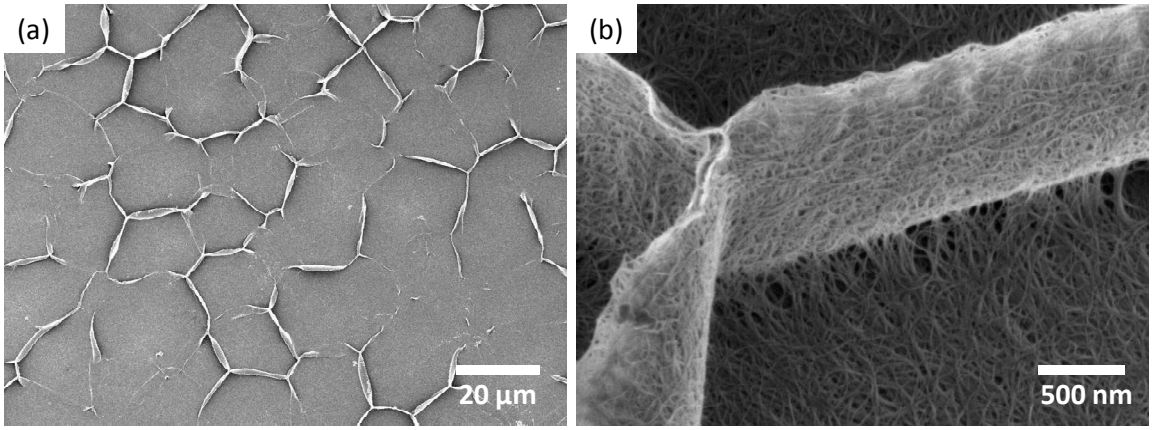

Figure S3-1. SEM images the μ-HN after acid doping. (a) Long-range morphology. (b) Magnified image of the wall in the μ-HN.

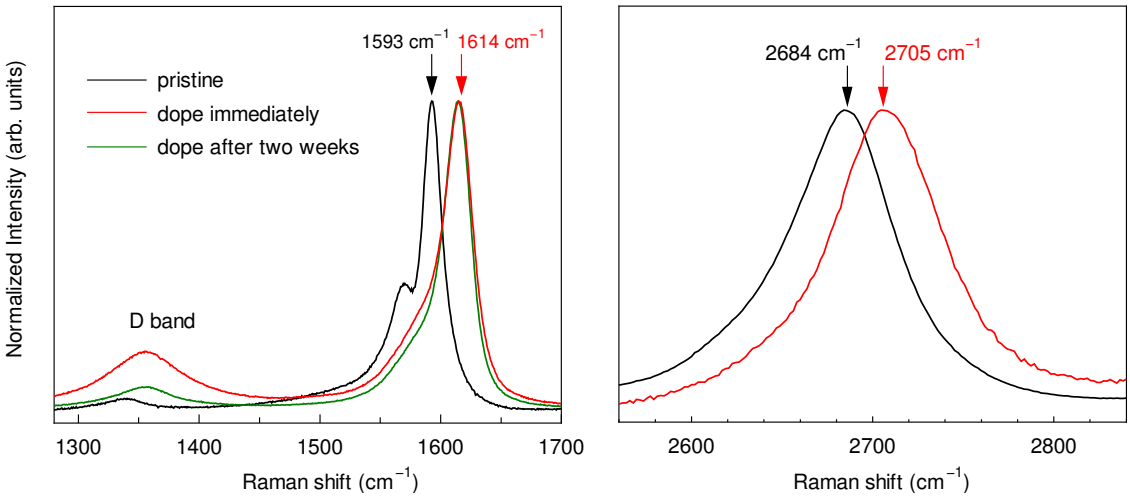

Figure S3-2. Raman spectra of pristine and nitric acid treated samples. Spectra of the treated samples were measured immediately after the samples were completely dried.

S4. Wavelength dependence of photocurrent generation

The spectrum responses (SM-250TF, Bunkoukeiki Co. Ltd) of both SWNT-Si solar cell and Si *p-n* junction solar cell (Si photodiode S1337, Hamamatsu Photonics K.K.) were obtained to discuss the wavelength dependence of the photocurrent generation. As shown in Figure S4, there is almost no external quantum efficiency when the photon energy is smaller than the silicon band gap (~1100 nm) for the SWNT-Si solar cell. Moreover, the SWNT-Si solar cell showed a similar shape as the conventional Si *p-n* junction solar cell. No obvious correlation between the SWNT absorption and the SWNT-Si spectrum response was observed in the 300 nm ~ 1150 nm range. This may be attributed to that the diameter of the SWNTs used in this research is around 2 nm, so that the main absorption peak E_{11} is around 2400 nm wavelength in the infrared region. This result further supports that the SWNT-Si solar cell is inversion type solar cell.

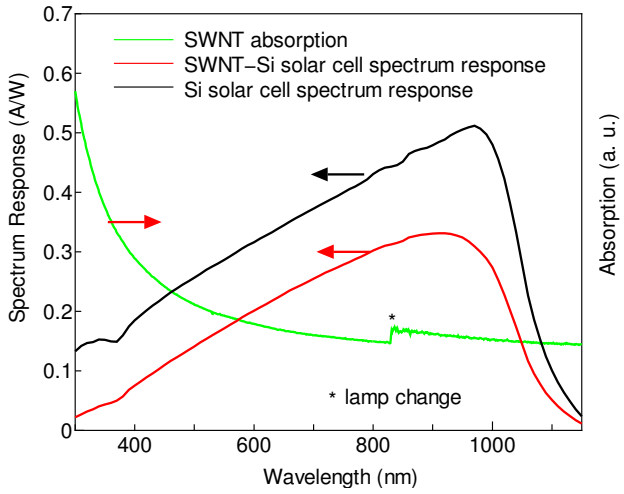

Figure S4. External quantum efficiency of the SWNT-Si solar cell and Si solar cell (left y axis), as well as the absorption spectrum of the SWNT therein (right y axis).

Reference

S1. Zhang, Z.; Einarsson, E.; Murakami, Y.; Miyauchi, Y.; Maruyama, S. Polarization Dependence of Radial Breathing Mode Peaks in Resonant Raman Spectra of Vertically Aligned single-Walled Carbon Nanotubes. *Phys. Rev. B* **2010**, *81*, 165442.

S2. Futaba, D. N.; Hata, K.; Yamada, T.; Hiraoka, T.; Hayamizu, Y.; Kakudate, Y.; Tanaike, O.; Hatori, H.; Yumura, M.; Iijima, S. Shape-Engineerable and Highly Densely Packed Single-Walled Carbon Nanotubes and Their Application as Super-Capacitor Electrodes. *Nat. Mater.* **2006,** *5*, 987-994.

S3. De Volder, M.; Hart, A. J. Engineering Hierarchical Nanostructures by Elastocapillary Self-Assembly. *Angew. Chem., Int. Ed.* **2013**, *52*, 2412-2425.

S4. Zhou, W.; Vavro, J.; Nemes N. M.; Fischer, J. E.; Borondics, F.; Kamarás, K.; Tanner, D. B. Charge Transfer and Fermi Level Shift in p-doped Single-Walled Carbon Nanotubes. *Phys. Rev. B* **2005**, *71*, 205423